DOI: 10.1002/adom.201800203

Article type: Full paper

Investigating the onset of the strong coupling regime by fine-tuning the Rabi splitting in multi-layer organic microcavities

*Laura Tropf and Malte C. Gather**

L. Tropf, Prof. M. C. Gather

Organic Semiconductor Centre, SUPA, School of Physics and Astronomy, North Haugh, St Andrews, KY16 9SS, United Kingdom

E-mail: mcg6@st-andrews.ac.uk

Keywords: polaritons, small molecules, light-matter coupling, excitons

ABSTRACT

Given the prevalence of disorder in many organic semiconductors, the applicability of simple models to describe their behavior in the strong coupling regime, like the two-level coupled oscillator, is not evident. Here, the validity of the two-level coupled oscillator model and the simple dependence of the coupling strength on the number of absorbers and the electric field is tested experimentally in metal-clad microcavities containing a disordered film of small molecules. Multi-layer microcavities are produced by combining different thin film deposition techniques. These allow for isolating the relevant parameters and thus to confirm the coupling strength is proportional to (1) the square root of the number of absorbers and (2) the amplitude of the electric field. By changing either of these two parameters, the microcavities are shifted from the weak to the strong coupling regime. Moreover, careful analysis reveals that there is a threshold coupling strength for the onset of the Rabi splitting. Two independent investigations show that this threshold is comparable to the losses in the cavities. These results validate the coupled two-level Hamiltonian for microcavities containing disordered organic semiconductors, even though the assumption of a single exciton level represents a strong simplification for these systems.

1. Introduction

Strong interactions between cavity photons and excitons give rise to mixed light-matter quasiparticles called exciton-polaritons. Their properties are a mixture of the properties of their constituents and are tunable to a certain extent. The combination of light mass (inherited from the photon), strong non-linearities (inherited from the exciton) and mostly short lifetimes (due to the leakage of photons from the cavity) have made them an exciting playground, for instance for non-equilibrium dynamics of quantum fluids.[1–11] In addition, the ability to control both the light and the matter part of the strongly coupled system gives rise to new devices like all optical transistors, optical amplifiers or low power spin switches.[12–14]

Using polaritons for applications requires them to persist up to room temperature, which is not possible in many inorganic materials as their exciton binding energies are too low. Other classes of materials, like organic semiconductors or nanomaterials, exhibit binding energies of the order of 0.5 eV, which renders them promising candidates for polariton devices.[15] While research on nanomaterials for polariton applications is still relatively young,[16,17] many milestones in (inorganic) polariton research, like superfluidity, condensation or confinement, have now been demonstrated in organic systems as well.[4,6,10,11,18] Moreover, some aspects of the strongly coupled could system enhance the properties of conventional organic semiconductor devices. For instance, some devices might exploit the angle-independent emission from the lower polariton branch of ultrastrongly coupled organic LEDs and others could benefit from a polariton-mediated improvement in transport properties.[19–22]

While the theoretical opportunities are vast, major challenges like electrical pumping of a polariton condensate or simple, versatile confinement techniques have yet to be overcome. On a microscopic and more fundamental level, using organic semiconductors for strong coupling

poses questions, like “At which level does the inhomogeneous linewidth of the exciton distort the two-level picture?” or “Do basic relations derived for idealized systems still hold for these materials?” For example, experiments found the two-level model to be ambiguous for organic semiconductors with (inhomogeneously) broad absorption and thus its applicability to be limited.[23] Other experiments, in contrast, have looked into validating the form of the coupling strength as derived for an ideal dipole coupled to a photon field. They confirmed that the coupling strength depends on the oscillator strength and the mode volume.[24] It follows from cavity quantum electrodynamics that the coupling strength is proportional to the electric field present. Experiments verifying this prediction for organic semiconductors used J-aggregate films in a dielectric-metal and in an all-metal cavity.[25,26] However, J-aggregates represent a particular class of organic semiconductors with a well-defined dipole – thus it is not evident whether this result can be transferred to more common organic materials which often have a broad absorption spectrum due to high degrees of disorder.

There have also been reports on the dependence of the coupling strength on the number of absorbers in organic materials, studying the Rabi splitting as a function of the exciton concentration.[27,28] Changing the concentration of an organic emitter in a host, however, will not only affect the number of absorbers. Energy transfer processes between the molecules will be altered as well (depending on the specific system, even severely), which is manifested for example in a strong dependence of the luminescence quantum yield on the concentration. The only studies we are aware of, which relate the Rabi splitting to the number of absorbers at constant concentration, were qualitative and have been performed on inorganic semiconductors.[29,30] One reason that no comparable study has been performed on organic materials yet may be the fabrication methods used for organic microcavities. These render an

independent variation of the thickness of the active material and other cavity parameters challenging.

Here, we report on a detailed experimental and quantitative study investigating the validity of the linear dependence of the coupling strength on (1) the square root of the number of absorbers and (2) the amplitude of the electric field. We use a low-molecular weight organic semiconductor and combine several vacuum thin film deposition techniques to gain maximum control over the structures of our samples, both in terms of accuracy of layer thickness and flexibility in choosing the layer sequence. This enables us to independently change the cavity thickness and organic film thickness, or even the overlap between the absorbers and the electric field. We confirm that the coupling strength is proportional to the square root of the number of absorbers and to the amplitude of the electric field. Our data also enable us to investigate the threshold for the onset of the Rabi splitting experimentally and quantitatively - to our knowledge for the first time. We determine this threshold coupling strength from two independent experimental approaches; changing the thickness of the organic film yields $g_{\mathrm{thr}}^{d\mathrm{org}} = 0.10 \pm 0.02$ eV and changing the overlap of an organic film of constant thickness with the electric field yields $g_{\mathrm{thr}}^{\mathrm{OVL}} = 0.07 \pm 0.03$ eV. Both values are in decent agreement with the independently estimated prediction of a two level model ($g_{\mathrm{thr}}^{\mathrm{theo}} = 0.07$ eV).

After a short introduction to the coupled two-level model, we present our experimental results investigating the Rabi splitting as a function of absorbers and as a function of the overlap between excitons and electric field. In the final section of the paper, we use these different studies to demonstrate the onset of the Rabi splitting at non-zero values of the coupling strength.

2. Background: How to access the coupling strength directly

Solving the Hamiltonian of an excited state X (with energy E_x and spontaneous relaxation rate $\gamma_x/\hbar$) coupled with coupling strength g to a photonic cavity mode C (with energy E_c and photon loss rate $\gamma_c/\hbar$) yields the eigenenergies of the resulting quasiparticles, the upper and lower polariton (UP and LP, respectively):

$$E_{UP/LP} = \frac{(E_x + E_c) - i(\gamma_x + \gamma_c)}{2} \pm \frac{1}{2}\sqrt{4g^2 + [(E_x - E_c) + i(\gamma_x - \gamma_c)]^2}\,. \quad (1)$$

At the point of resonance, $E_c - E_x = 0$, the splitting between the modes, $\Delta E_{UP,LP}$, becomes minimal and Equation 1 simplifies to the so-called Rabi splitting, $\hbar\Omega$, which is considered a measure of the coupling strength,

$$\hbar\Omega = \sqrt{4g^2 - (\gamma_x - \gamma_c)^2}\,. \quad (2)$$

From Equation 2 it is clear, however, that $\hbar\Omega$ is no exact measure of the coupling strength g. Instead, losses in the form of spontaneous exciton relaxation, γ_x, and due to leakage of photons out of the cavity, γ_c, lead to a reduction of the observed splitting for a given coupling strength. In particular, the Rabi splitting will only set in for coupling strengths fulfilling

$$g_{thr} > \frac{|\gamma_x - \gamma_c|}{2}. \quad (3)$$

The coupling strength is determined by parameters of both the cavity photons – like the mode volume V or the amplitude of the electric field A – and the excitons, namely their transition

dipole moment (or molecular oscillator strength f) and the number of absorbers, N. This can be summarized as $g \propto A \times \sqrt{Nf/V}$.[31,32] The coupling strength is not directly experimentally accessible, though; we can only measure the mode splitting (Equation 1) or the Rabi splitting (Equation 2). We can, however, deduce the dependence of the coupling strength on the investigated parameters by determining the mode splitting as a function of these parameters. We then fit the experimental data and account for the exact form of the energy splitting in the fit.

Aiming at examining the dependence of the coupling strength on the number of absorbers, we study the dependence of the Rabi splitting on the thickness of the organic film, d, which is possible because $d \propto N$. Assuming the validity of Equation 2, our experimental data are tested against a fit function of the form

$$g \propto \sqrt{N} \;\leftrightarrow\; \hbar\Omega(d) = \sqrt{a_N \times d - b_N}, \tag{4}$$

where a_N and b_N are fit parameters. We emphasize that this differs from the generally assumed $\hbar\Omega \propto \sqrt{N}$, which is usually investigated.[17,24,27]

Similarly, we can verify the dependence of the coupling strength on the electric field amplitude. For technical reasons, we do not measure the Rabi splitting in this case, but the mode splitting at constant detuning, so that

$$g \propto A \;\leftrightarrow\; \left[\Delta E_{\mathrm{UP,LP}}(A)\right]^2 = a_A \times A^2 - b_A. \tag{5}$$

Again, a_A and b_A are fit parameters, where

$$b_A = (E_\mathrm{x} - E_\mathrm{c})^2 - (\gamma_\mathrm{x} - \gamma_\mathrm{c})^2 + 2i(E_\mathrm{x} - E_\mathrm{c})(\gamma_\mathrm{x} - \gamma_\mathrm{c}). \tag{6}$$

Both fit functions distinguish clearly between the Rabi/mode splitting and the coupling strength, which gives rise to the offsets b_N and b_A in Equation 4 and 5, respectively. This has one further advantage: according to Equation 3, we can extract one value- for the threshold for strong coupling from each investigation described above, i.e. from b_N and b_A, respectively. An independent estimate of the losses γ_{x} and γ_{c} then enables us to verify Equation 3 and thus the validity of the coupled oscillator model.

3. Results and discussion

We use the small molecule 2,3,6,7-tetrahydro-1,1,7,7,-tetramethyl-1H,5H,11H -10-(2-benzothiazolyl)quinolizino-[9,9a,1gh]coumarin (C545T) as active, organic material for performing the investigations described above. C545T has been shown to be an efficient organic emitter for organic LEDs and lasers.[33,34] Its chemical structure is given in **Figure 1**(a) together with the spectrally resolved refractive index and extinction coefficient obtained by ellipsometry measurements. The extinction displays a broad peak, which can be decomposed into four overlapping vibronic replica. This decomposition indicates that the lowest energy exciton is centered at $E_{\mathrm{x},0} = (2.51 \pm 0.02)$ eV and the first vibronic replica at $E_{\mathrm{x},1} = (2.70 \pm 0.02)$ eV. The refractive index and extinction coefficient are fed into a transfer matrix (TM) algorithm, which is used for analyzing the experimental results. Independently measured transmittance spectra, T, of C545T films of different thickness, which relate to the absorbance A via $A = -\log_{10}(T)$, confirm the measurements of the optical constants and are shown in the supplementary information (Figure S1).

In order to test the validity of Equation 4 and 5, we designed two sample series named *dorg* (varying the thickness of the organic material) and *OVL* (changing the overlap between the organic film and the electric field, OVL for overlap). They were used to study the coupling strength as a function of the number of absorbers and of the electric field, respectively. All samples were metal-clad cavities, inside which the organic material was additionally sandwiched between two SiO_2 spacer layers, as sketched in Figure 1(b). Since SiO_2 is transparent in the investigated spectral range, it was used to provide an additional degree of freedom for the design of the samples. This enabled us either to change the cavity thickness – and thus the detuning – independently of the organic film thickness (*dorg* series) or to change solely the position of an organic film of constant thickness (*OVL* series).

3.1. Coupling strength as a function of the number of absorbers

The *dorg* series consisted of $\lambda/2$-cavities (i.e. cavities with an optical thickness of $\lambda/2$ such that the fundamental mode roughly matches the exciton energy) with organic films of different thicknesses placed in the center as sketched in Figure 1(b). These samples were grouped in sets of cavities with constant thickness of the organic film but different optical thicknesses. The organic film thickness was varied between different sets.

The experimental reflectance spectra of three selected sets of four cavities with positive and negative detunings are presented in **Figure 2** (upper row). The thickness of the organic film and of the SiO_2 spacer layers is determined for each cavity by fitting transfer matrix (TM) calculations to the measured spectra. The resulting values are given in the respective panels of Figure 2. Empty cavities, i.e. cavities with no organic material inside, show a single dip in reflectance across the investigated spectral range, which is attributed to the cavity mode. On

introducing a C545T film into the cavity, two dips appear at either side of the exciton energy of C545T. This is the characteristic signature of splitting into UP and LP. The magnitude of this splitting, i.e. the separation between the two dips, is furthermore dependent on the organic film thickness as can be seen by comparing Figure 2(b) and (c).

The lower row of Figure 2 shows TM calculations of reflectance spectra for cavities with the same C545T thicknesses as in the upper row but with a continuous variation in the optical thickness of the cavity (achieved by adjusting the spacer layer thickness in the TM calculations accordingly). The calculations are in good agreement with the mode positions found experimentally (c.f., grey symbols in lower row of Figure 2). In order to quantify the difference between the cavity sets, we extracted the Rabi splitting $\hbar\Omega$ from each calculated reflectance map by reading off the minimum splitting between the UP and LP mode.

The relationship between Rabi splitting and C545T thickness is analyzed in **Figure 3**(a), where each black symbol represents one set of cavities (i.e. one film thickness of C545T) and the corresponding TM calculation. These data were then fitted according to Equation 4 to test if the coupling strength was proportional to the square root of the number of absorbers. The fit was performed on all data points with C545T thicknesses $d > 4$ nm, since below that threshold, the overlap of UP and LP obscured any double-dip features (see supplementary information). Despite a reasonable coefficient of determination, $R^2 = 0.961$, a systematic deviation of the data from the fit is apparent. We suspect that this difference is caused by the non-homogeneous electric field inside the cavity, which is tested in the following section.

3.2. Coupling strength as a function of the electric field

The intra-cavity electric field has nodes at each mirror and (at least for $\lambda/2$-cavities) one antinode in the center of the cavity, as illustrated in the middle panel of Figure 3. Thus, the thinner the organic films in the center of the cavity are, the higher is the average electric field they are exposed to. This effect could cause the deviation of the experimental data from Equation 4 due to the dependence of the coupling strength on the electric field amplitude. Correcting the physical thickness of the C545T film for the relative overlap with the electric field indeed yields a better overall agreement between the experimental data and the fit, resulting in a higher goodness of fit, $R^2 = 0.989$ (Figure 3(b) and supplementary information). Hence, we conclude that it is important to consider the overlap of the organic film with the electric field to accurately calculate the expected Rabi splitting for a given cavity structure.

The second sample series was designed to isolate and thus verify this effect: In these cavities, the overlap between the electric field and the organic film is the only variable. This was achieved by placing C545T films of the same thickness, $d = 42$ nm, at different positions within an approximately zero-detuned λ-microcavity, as illustrated in **Figure 4**(a). We adjusted the SiO_2 spacer thicknesses in order to have a minimal (OVL0) to maximal (OVL3) overlap between the organic material and the electric field of the cavity mode. An empty reference cavity of the same optical thickness but without any organic material was also produced (OVLx).

Figure 4(b) shows the experimental reflectance spectra of all cavities from the *OVL* series. All spectra were recorded at the same detuning as can be verified from the uncoupled fundamental mode of the cavity, which is at the same energy for all cavities. The spectra

clearly show an increase of the mode splitting with increasing overlap between the active film and the electric field, i.e. from OVL0 to OVL3, up to $\Delta E_{\mathrm{UP,LP}}^{OVL3} = 0.57$ eV. By contrast, the reflectance spectrum of the sample with the least overlap (OVL0) is very similar to that of the uncoupled reference sample (OVLx) and does not show any mode splitting. We emphasize that this shift between weak and strong coupling regime is merely driven by the overlap of the electric field with absorbers in the cavity; all other parameters, including the film thickness (i.e. number of absorbers), are kept constant.

A comparison to TM calculations reveals that this behavior is expected for a thin organic film at different positions in the microcavity (Figure 4(c)). Additionally, the calculations indicate that the mode splitting is not mirror-symmetric around the center of the cavity. We confirmed the asymmetry experimentally by fabricating a cavity, which nominally had the same overlap as OVL1 but was positioned in the lower half of the cavity (OVL1m, see supplementary information). Its reflectance spectrum differed from that of OVL1, as predicted by the TM calculations. Further TM calculations show that the asymmetry is not caused by the asymmetry of the mirrors (20 vs 150 nm thickness of the Al layer). Instead, it is a consequence of the intrinsically non-symmetric measurement of the reflectance; calculated transmittance spectra are fully symmetric (see supplementary information).

Next, we quantitatively study the observed mode splittings as a function of the average electric field amplitude to which the organic films are exposed (Figure 4(d)). Note that the cavities are slightly detuned (we are thus not studying the Rabi splitting) and that we converted the different film positions into average electric field amplitudes using TM calculations. By fitting the experimental data with a function of the form of Equation 5, we can test the two assumptions made in this equation: a direct proportionality of the coupling

strength to the electric field and the validity of the two-level model. As can be seen in Figure 4(d), the fit describes the data very well ($R^2 = 0.994$, see supplementary information). This confirms that the simple relationship of the coupling strength being proportional to the electric field amplitude also holds for the real, disordered system of organic microcavities.

3.3. Threshold for the onset of strong coupling

As discussed above, the solution of the two-level Hamiltonian predicts a threshold for the onset of the strong coupling regime that depends on the losses of the system (Equation 3). Strong coupling only occurs for coupling strengths $g > \frac{|\gamma_x - \gamma_c|}{2}$. The photonic decay rate at the energy of the uncoupled exciton, $E_x \approx 2.6$ eV, was estimated from the spectral width of a bare cavity photon mode, yielding $\gamma_c = 0.13$ eV. For organic semiconductors, radiative lifetimes are $\gg 1$ ps, i.e. $\gamma_x \ll 10^{-4}$eV. The losses of the system are thus entirely dominated by photon leakage from the microcavity, $\gamma_x \ll \gamma_c$, and we therefore expect a threshold for the onset of the Rabi splitting at $g_{thr} = \gamma_c/2 = 0.07$ eV.

We can now use both sample series, *dorg* and *OVL*, to determine the threshold of the strong coupling regime in two independent ways. From the *dorg* series with varying thickness of the organic layer, the threshold follows from the fitting parameters as $g_{thr}^{dorg} = \sqrt{b_N}/2 = (0.10 \pm 0.02)$ eV (see Equation 4). For the *OVL* series, the threshold can only be calculated indirectly from the fitting parameter b_A in Equation 5 as these samples have a finite amount of detuning, $\delta = E_x - E_c = 0.07$ eV (see Experimental Section). Since the analysis relies only on the mode positions, which correspond to the real part of b_A, we do not need to consider dissipation and we can neglect the imaginary term $i \times 2(E_x - E_c)(\gamma_x - \gamma_c)$ in Equation 6 to obtain:

$$g_{\mathrm{thr}}^{\mathrm{OVL}} = \frac{\sqrt{(E_{\mathrm{x}}-E_{\mathrm{c}})^2 - b_A}}{2} = (0.07 \pm 0.03)\ \mathrm{eV}. \quad (9)$$

Both independently determined values for the threshold are close to the value expected from solving the coupled oscillator model. These results show that losses indeed do lead to a non-zero threshold for the onset of the strong coupling regime. In metal-clad cavities, which are widely used for studying organic polaritons, this threshold turns out to be non-negligible.

4. Conclusion

In summary, we have experimentally studied the effect of two parameters on the Rabi splitting: the thickness of the organic film (i.e. number of absorbers in the cavity) and the overlap between absorbers and electric field. In contrast to earlier studies, these investigations required the cavity thickness to be independent of the thickness of the organic film, which we achieved by combining different thin film deposition techniques (sputtering and thermal evaporation). The control over the heterostructure microcavities produced in this way gave us the necessary, additional degree of freedom in sample design. Using these structures, we demonstrated two different ways of transitioning between the weak and the strong coupling regime. We quantitatively confirmed the proportionality of the coupling strength on the electric field amplitude and on the square root of the number of absorbers for an organic semiconductor with strong disorder.

Additionally, we showed that in agreement with theory, the Rabi splitting has a defined threshold that depends on the losses of the system. The two-level model more precisely predicts this threshold to be proportional to the difference in losses of the excitonic and photonic constituent. To verify this, however, one would need to design a system where the

photonic and excitonic decay rates are comparable (and can possibly be tuned). In our system, – and likely in most other organic-filled microcavities with Q-factors of $Q < 10^5$ – photon leakage from the cavity strongly dominates the losses so that we cannot experimentally access the exact form of the threshold (Equation 3). We were able to demonstrate, though, that the magnitude of the strong coupling threshold is similar to these dominant photonic losses (divided by two). All our findings thus indicate that a simple two-level Hamiltonian can also be used to describe strong coupling in organic materials with a broad absorption.

5. Experimental Section

Sample fabrication: Bottom mirrors of 150 ± 15 nm Al were sputtered on glass substrates using DC sputtering (Nexdep 030 DC/RF sputtering system by Angstrom Engineering). SiO_2 spacer layers of different thicknesses were sputtered from a SiO_2 target using RF magnetron sputtering. Both sputtering processes use an Ar only plasma. C545T (Lumtec) was thermally evaporated (Evovac deposition system by Angstrom Engineering). The top SiO_2 spacer (again with different thicknesses) and semitransparent Al mirror (20 ± 2 nm) were sputtered as specified above. All films were deposited at ambient temperature to avoid damage to the C545T film. Samples were either in high vacuum or in an oxygen and moisture-free glovebox environment throughout the fabrication.

Sample characterization: The complex refractive index of C545T was obtained from neat films deposited on Si substrates using variable angle spectroscopic ellipsometry (M-2000DI by J.A. Woollam Co., Inc.). The optical constants were used in a TM algorithm based code to design the cavities used in this study. The properties of the microcavities were probed through

the semitransparent top mirror using p-polarized white light reflectance under angles $\theta > 45°$ (M-2000DI). TM-calculated reflectance spectra were then fitted to the experimental spectra to extract the thicknesses of the individual layers. For the *dorg* series, both the spacer layer thickness and the organic thickness were used as fitting parameters and the organic film was assumed to be located at the center of the microcavity. For the *OVL* series, the C545T thickness was not a fit parameter but instead assumed to be $d = 42$ nm for all samples in the series, as determined by ellipsometry on a control film that was evaporated on a bare substrate at the same time. The total thickness of the top and bottom SiO_2 spacer was a fit parameter, while their ratio was assumed to be the ratio measured by QCM.

Overlap of electric field and organic film: The distribution of the electric field amplitude in an empty cavity (SiO_2 only) was calculated at the energy of the uncoupled mode using the TM algorithm. The optical thickness of the calculated cavity was matched to that of the relevant experimental samples. From the (optical) thickness and position of the organic film, the average field $\bar{A}$ to which the C545T molecules are exposed was calculated. In the sample series *dorg*, the correction to the thickness of the C545T film for the field overlap was made as $d_{\mathrm{C545T}} \times \bar{A}/\bar{A}_{\mathrm{max}}$, where $\bar{A}_{\mathrm{max}}$ is the maximum average field amplitude observed for any of the investigated microcavities.

Detuning of cavities in OVL series: The energy of the cavity photon was determined from the energy of the uncoupled cavity mode in OVL0 (i.e., the sample which did not show any mode splitting) to be $E_C = 2.52$ eV. The energy of the exciton was determined from TM simulations as the midpoint between UP and LP at the splitting minimum of a microcavity

with a similar structure (i.e., 40 nm of C545T in the center of the cavity). This yielded $E_X = 2.59$ eV, so that the detuning is calculated to be $\delta = E_x - E_c = 0.07$ eV.

Acknowledgements

We thank J. Keeling for inspiring discussions. This research was financially supported by the European Research Council under the European Union's Horizon 2020 Framework Programme (FP/2014-2020)/ERC Grant Agreement No. 640012 (ABLASE), the Volkswagen Foundation (93404), and the Scottish Funding Council (through SUPA). L.T. acknowledges the studentship funding through the EPSRC CM-CDT (EP/L015110/1).

Received: ((will be filled in by the editorial staff))

Revised: ((will be filled in by the editorial staff))

Published online: ((will be filled in by the editorial staff))

References

[1] J. Kasprzak, M. Richard, S. Kundermann, A. Baas, P. Jeambrun, J. M. J. Keeling, F. M. Marchetti, M. H. Szymańska, R. André, J. L. Staehli, V. Savona, P. B. Littlewood, B. Deveaud, L. S. Dang, *Nature* **2006**, *443*, 409.

[2] K. G. Lagoudakis, M. Wouters, M. Richard, A. Baas, I. Carusotto, R. André, L. S. Dang, B. Deveaud-Plédran, *Nat. Phys.* **2008**, *4*, 706.

[3] A. Amo, S. Pigeon, D. Sanvitto, V. G. Sala, R. Hivet, I. Carusotto, F. Pisanello, G. Lemenager, R. Houdre, E. Giacobino, C. Ciuti, A. Bramati, *Science* **2011**, *332*, 1167.

[4] J. D. Plumhof, T. Stöferle, L. Mai, U. Scherf, R. F. Mahrt, *Nat. Mater.* **2013**, *13*, 247.

[5] K. S. Daskalakis, P. S. Eldridge, G. Christmann, E. Trichas, R. Murray, E. Iliopoulos, E. Monroy, N. T. Pelekanos, J. J. Baumberg, P. G. Savvidis, *Appl. Phys. Lett.* **2013**, *102*, 101113.

[6] K. S. Daskalakis, S. A. Maier, R. Murray, S. Kéna-Cohen, *Nat. Mater.* **2014**, *13*, 271.

[7] C. Sturm, D. Solnyshkov, O. Krebs, A. Lemaître, I. Sagnes, E. Galopin, A. Amo, G. Malpuech, J. Bloch, *Phys. Rev. B* **2015**, *91*, 155130.

[8] S. Klembt, E. Durupt, S. Datta, T. Klein, A. Baas, Y. Léger, C. Kruse, D. Hommel, A. Minguzzi, M. Richard, *Phys. Rev. Lett.* **2015**, *114*, 186403.

[9] N. Bobrovska, M. Matuszewski, K. S. Daskalakis, S. A. Maier, S. Kéna-Cohen, *ACS Photonics* **2017**, *5*, 111.

[10] G. Lerario, A. Fieramosca, F. Barachati, D. Ballarini, K. S. Daskalakis, L. Dominici, M. De Giorgi, S. A. Maier, G. Gigli, S. Kéna-Cohen, D. Sanvitto, *Nat. Phys.* **2017**, *13*, 837.

[11] G. Lerario, D. Ballarini, A. Fieramosca, A. Cannavale, A. Genco, F. Mangione, S. Gambino, L. Dominici, M. De Giorgi, G. Gigli, D. Sanvitto, *Light Sci. Appl.* **2016**, *6*, e16212.

[12] D. Ballarini, M. De Giorgi, E. Cancellieri, R. Houdré, E. Giacobino, R. Cingolani, A. Bramati, G. Gigli, D. Sanvitto, *Nat. Commun.* **2013**, *4*, 1778.

[13] D. D. Solnyshkov, H. Terças, G. Malpuech, *Appl. Phys. Lett.* **2014**, *105*, 231102.

[14] A. Dreismann, H. Ohadi, Y. del Valle-Inclan Redondo, R. Balili, Y. G. Rubo, S. I. Tsintzos, G. Deligeorgis, Z. Hatzopoulos, P. G. Savvidis, J. J. Baumberg, *Nat. Mater.* **2016**, *15*, 1074.

[15] D. Sanvitto, S. Kéna-Cohen, *Nat. Mater.* **2016**, *15*, 1061.

[16] X. Liu, T. Galfsky, Z. Sun, F. Xia, E. Lin, Y.-H. Lee, S. Kéna-Cohen, V. M. Menon, *Nat. Photonics* **2014**, *9*, 30.

[17] A. Graf, L. Tropf, Y. Zakharko, J. Zaumseil, M. C. Gather, *Nat. Commun.* **2016**, *7*, 13078.

[18] D. Urbonas, T. Stöferle, F. Scafirimuto, U. Scherf, R. F. Mahrt, *ACS Photonics* **2016**, *3*, 1542.

[19] M. Mazzeo, A. Genco, S. Gambino, D. Ballarini, F. Mangione, O. Di Stefano, S. Patanè, S. Savasta, D. Sanvitto, G. Gigli, *Appl. Phys. Lett.* **2014**, *104*, 233303.

[20] C. R. Gubbin, S. A. Maier, S. Kéna-Cohen, *Appl. Phys. Lett.* **2014**, *104*, 233302.

[21] E. Orgiu, J. George, J. A. Hutchison, E. Devaux, J. F. Dayen, B. Doudin, F. Stellacci, C. Genet, J. Schachenmayer, C. Genes, G. Pupillo, P. Samorì, T. W. Ebbesen, *Nat. Mater.* **2015**, *14*, 1123.

[22] J. Feist, F. J. Garcia-Vidal, *Phys. Rev. Lett.* **2015**, *114*, 196402.

[23] R. F. Oulton, N. Takada, J. Koe, P. N. Stavrinou, D. D. C. Bradley, *Semicond. Sci. Technol.* **2003**, *18*, S419.

[24] P. A. Hobson, W. L. Barnes, D. G. Lidzey, G. A. Gehring, D. M. Whittaker, M. S. Skolnick, S. Walker, *Appl. Phys. Lett.* **2002**, *81*, 3519.

[25] P. Schouwink, H. . Berlepsch, L. Dähne, R. . Mahrt, *Chem. Phys.* **2002**, *285*, 113.

[26] S. Wang, T. Chervy, J. George, J. A. Hutchison, C. Genet, T. W. Ebbesen, *J. Phys. Chem. Lett.* **2014**, *5*, 1433.

[27] D. G. Lidzey, D. D. C. Bradley, M. S. Skolnick, T. Virgili, S. Walker, D. M. Whittaker, *Nature* **1998**, *395*, 53.

[28] J. A. Hutchison, T. Schwartz, C. Genet, E. Devaux, T. W. Ebbesen, *Angew. Chem.* **2012**, *124*, 1624.

[29] A. Tredicucci, Y. Chen, V. Pellegrini, M. Börger, L. Sorba, F. Beltram, F. Bassani, *Phys. Rev. Lett.* **1995**, *75*, 3906.

[30] S. Brodbeck, S. De Liberato, M. Amthor, M. Klaas, M. Kamp, L. Worschech, C. Schneider, S. Höfling, *Phys. Rev. Lett.* **2017**, *119*.

[31] V. Agranovich, M. Litinskaia, D. Lidzey, *Phys. Rev. B* **2003**, *67*, 085311.

[32] A. V. Kavokin, J. J. Baumberg, G. Malpeuch, F. P. Laussy, *Microcavities*, Oxford University Press, Oxford ; New York, **2007**.

[33] F. J. Duarte, L. S. Liao, K. M. Vaeth, A. M. Miller, *J. Opt. Pure Appl. Opt.* **2006**, *8*, 172.

[34] C. H. Chen, C. W. Tang, *Appl. Phys. Lett.* **2001**, *79*, 3711.

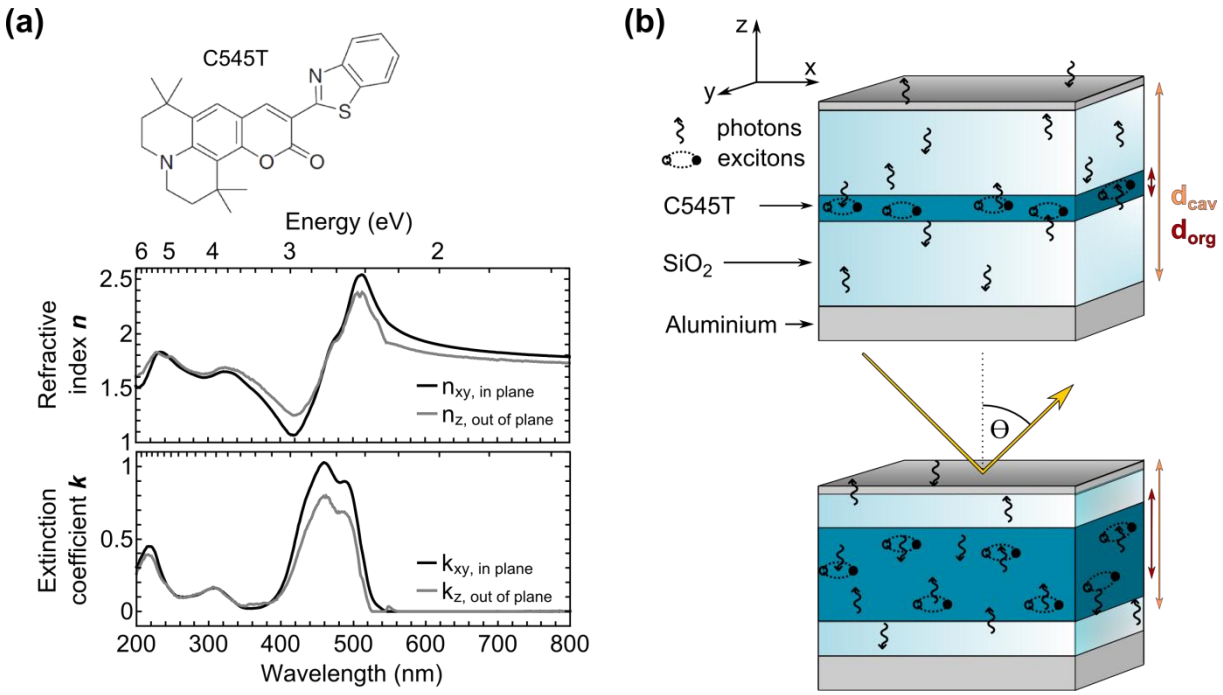

Figure 1. (a) Chemical structure, anisotropic refractive index *n* and extinction coefficient *k* of C545T. (b) Schematic illustration of cavities in *dorg* series used to investigate the influence of the number of absorbers on the coupling strength. In the aluminum-clad cavities, SiO_2 spacers allow for an independent variation of the organic film thickness and the cavity thickness.

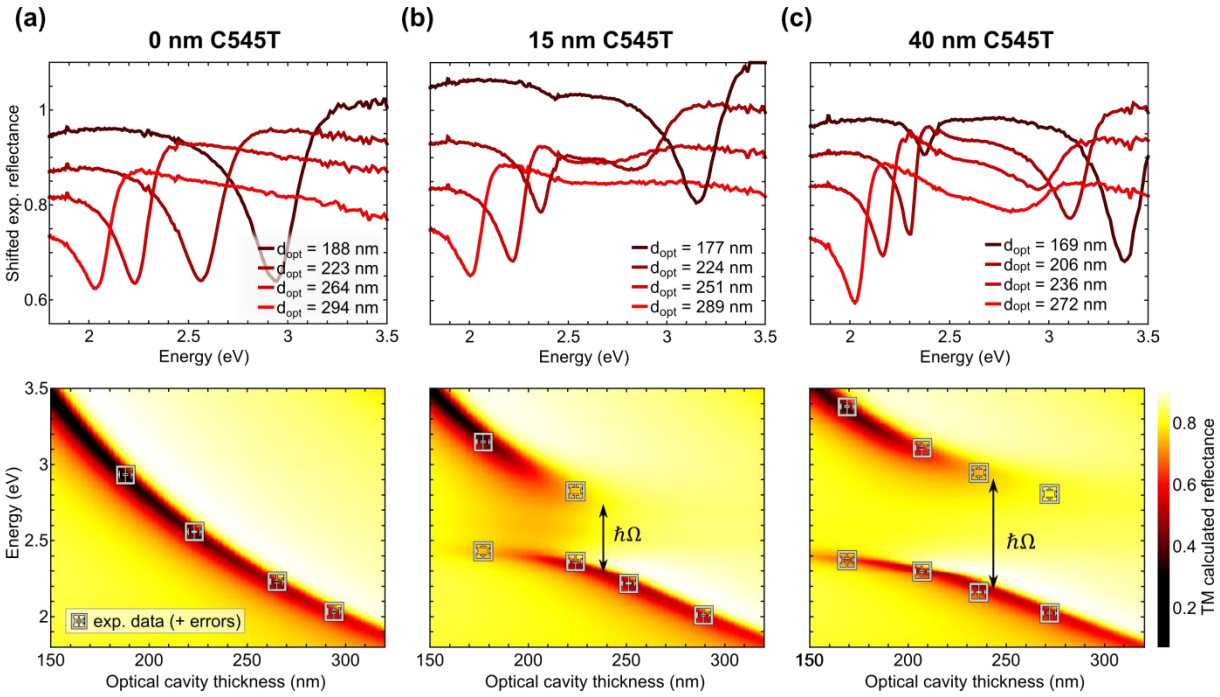

Figure 2. Reflectance of cavities with different total optical thicknesses, d_{opt}, for three different thicknesses of C545T (d_{C545T} = const. in each column): (a) $d_{C545T} = 0$ nm, (b) 15 nm, and (c) 40 nm. The upper row of panels shows experimental reflectance spectra. The lower row compares the experimental mode positions (grey symbols) with transfer matrix (TM) calculations for corresponding cavity structures with continuously varying optical thickness (background).

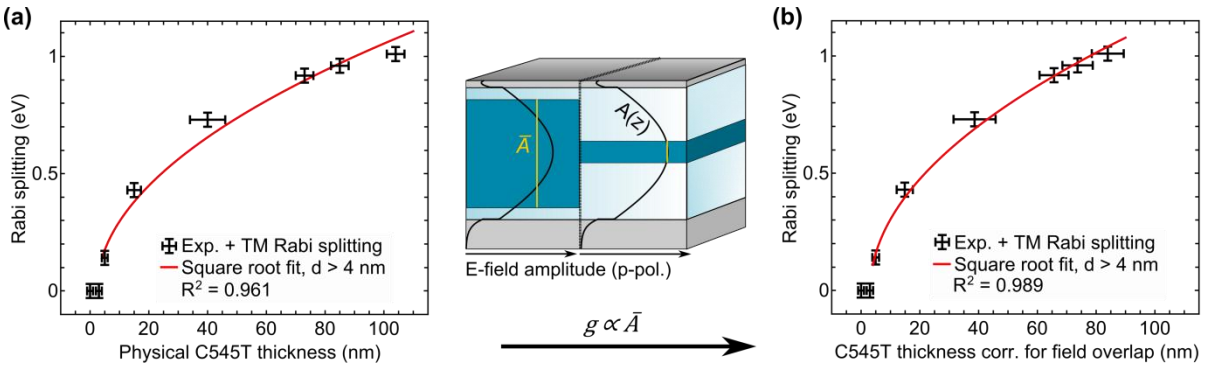

Figure 3. (a) Rabi splitting as a function of physical C545T thickness (black symbols) and square root fit, $\hbar\Omega = \sqrt{a_N d + b_N}$ (red line). The middle panel illustrates how the mean field amplitude $\bar{A}$ across the C545T film differs for different thicknesses of the C545T film (yellow lines). (b) Rabi splitting as a function of the C545T thickness corrected for different overlaps of the organic film with the electric field amplitude (black symbols). The square root fit (red line) yields a higher coefficient of determination, R^2, than in (a).

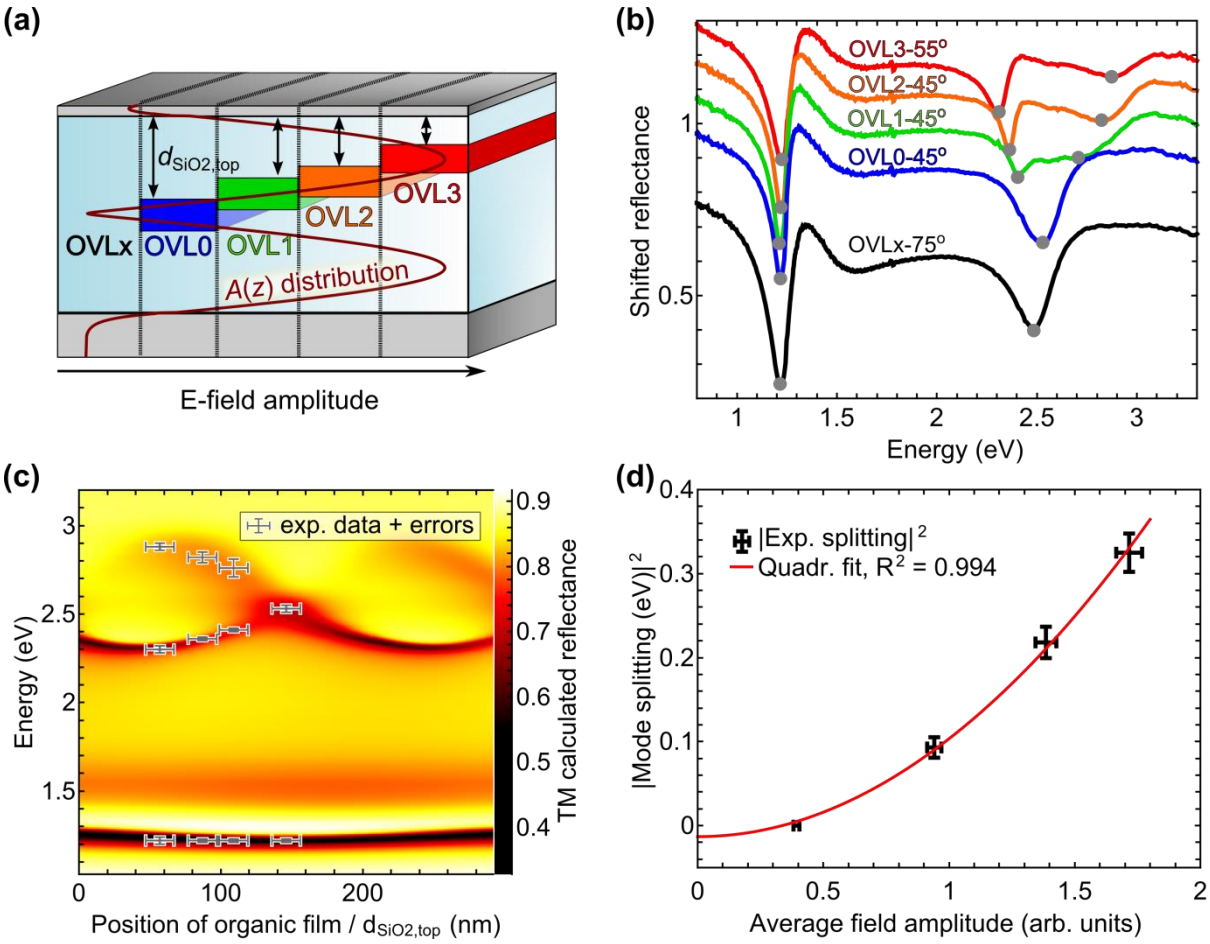

Figure 4. (a) Schematic illustration of the *OVL* series used to investigate the influence of the overlap between photonic mode and absorbers in cavity. Layers of identical C545T thickness are positioned at different locations across the cavity (increasing field overlap from sample OVL0 to OVL3). The reference cavity, OVLx, has no C545T layer. $d_{SiO2,\,top}$ refers to the thickness of the top SiO_2 layer, which defines the position of the organic film inside the cavity. (b) Reflectance spectra of the *OVL* series. Reflectance spectra were acquired at different angles of incidence (see legend) in order to tune the fundamental cavity mode to an energy of 1.21 eV for all samples, and thus obtain the same amount of detuning. Gray symbols indicate mode positions. (c) Comparison of experimental mode positions (gray symbols) with a TM calculation for corresponding cavity structures with a continuously varying location of the

C545T film (background). (d) Mode splitting extracted from the experimental reflectance spectra as a function of the average field amplitude to which the organic film is exposed (black symbols) and parabolic fit (red line).